LONG-RANGE SOUND PROPAGATION IN THE CANADA BASIN

Timothy F. Duda, Weifeng Gordon Zhang, Ying-Tsong Lin and Arthur E. Newhall

Woods Hole Oceanographic Institution, Woods Hole, MA, USA

Contact author Timothy Duda, WHOI AOPE Dept., Woods Hole, MA 02543, USA, v: 1-508 289 2495, tduda@whoi.edu

Abstract: *The existence of a sound duct created by the presence of waters of Pacific origin in the Canada Basin and Beaufort Gyre allows sound to travel great distances with little attenuation. However, the water mass layering that creates the duct varies in time and space, and the ducting effect also varies. Output from a surface-forced hydrodynamic model of the region is analyzed to learn about the formation and flow of the water masses, and about eddies and filaments that strengthen and weaken the duct. The model results are then used for broadband two-dimensional parabolic equation modeling of sound to learn about seasonal variation of propagation in the region, as well as statistics of propagation variability.*

Keywords: *Ocean dynamical modeling, Beaufort Gyre, Pacific Summer Water, sound channel*

1. INTRODUCTION

The Beaufort Gyre lies north of Alaska in the southern portion of the Canada Basin of the Arctic Ocean. The anticyclonic (clockwise) gyre structure arises from atmospheric forcing [1], and impacts the flow throughout the region of relatively fresh water inputs with Bering Strait origin. Observations show that a layer of warm and fresh Pacific Summer Water (PSW) can lie above a very persistent layer of cold fresh Pacific Winter Water (PWW), which in turn overlies salty Atlantic Water. This creates a PWW duct with a sound velocity minimum, lying at 75 to 250 m depth. A recent article presents a discussion of propagation in this duct [2]. Fig. 1 shows the duct structure in a transect with seven deep CTD stations by the Canada Institute of Ocean Sciences in 2017 [3]. Below 350 m depth sound speed increases, which means that all sound is surface interacting unless it is confined to the PWW duct.

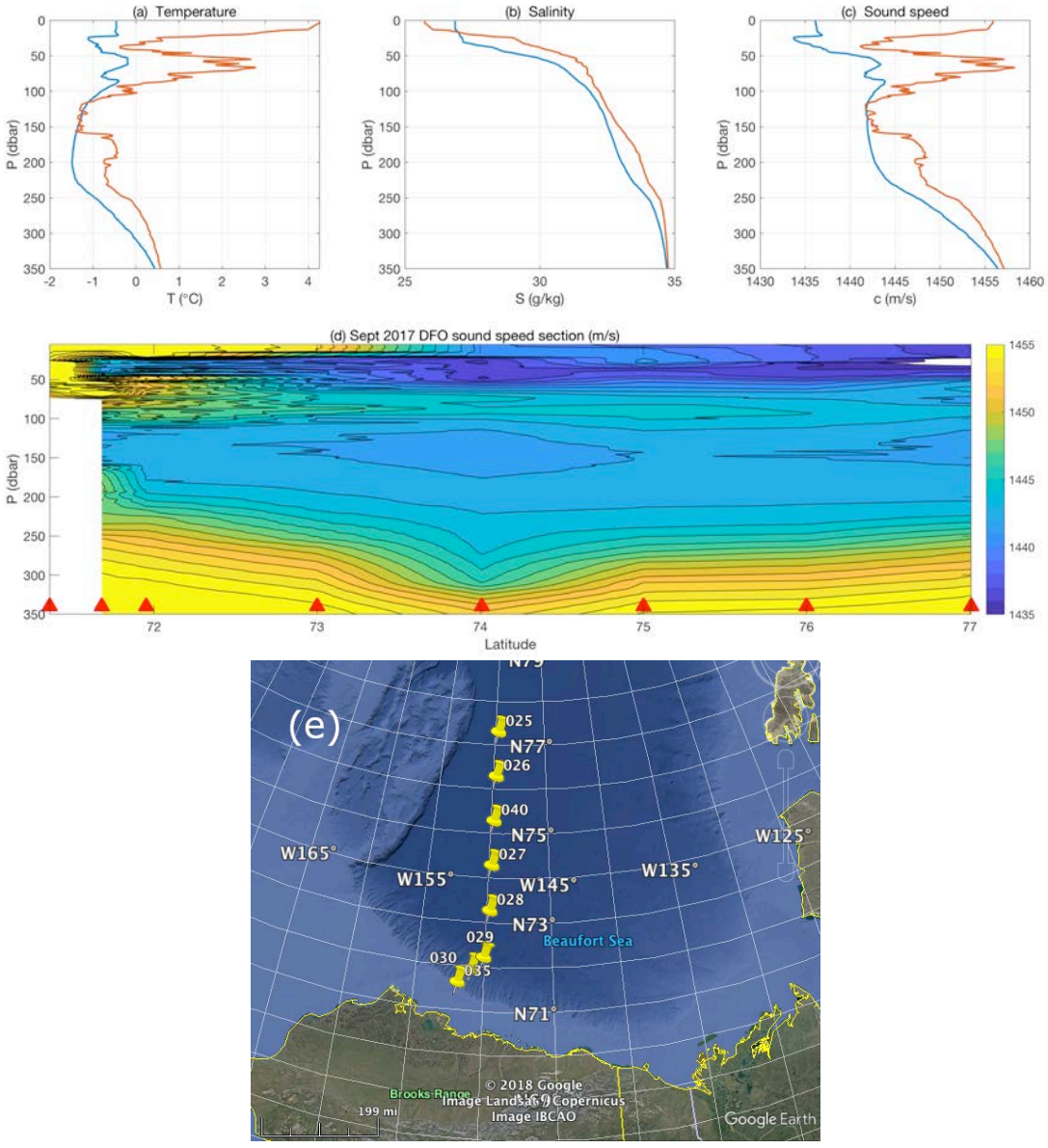

Fig 1: The Pacific Winter Water sound duct is shown. The top three panels show data from northern station 25 and southernmost deep station 30: (a) shows temperature, (b) shows salinity, and (c) shows sound speed. The center panel (d) shows sound speed in transect with 0.5 m/s contour interval. The lower panel (e) shows the station locations in the Canada Basin.

The duct is capped with warmer water in the south and is “stronger”, while it is weaker at the north. It appears to be continuous with this sparse sampling. In the northern five stations the sound speed minimum is near 1442 m/s and the duct top value is between 1444 and 1446.

In the next section, we present hydrodynamic model simulations for the area which show that the duct may be discontinuous. Evidence of duct discontinuity was found in the Canada Basin Acoustic Propagation Experiment (CANAPE) of Oct 2016 - Aug 2017, when sound propagating in the duct over hundreds of km in fixed paths showed time variability. In Section 3, acoustic propagation simulations made using the simulated duct conditions show potential effects of horizontal variations of the duct on long-range 200-Hz sound propagation.

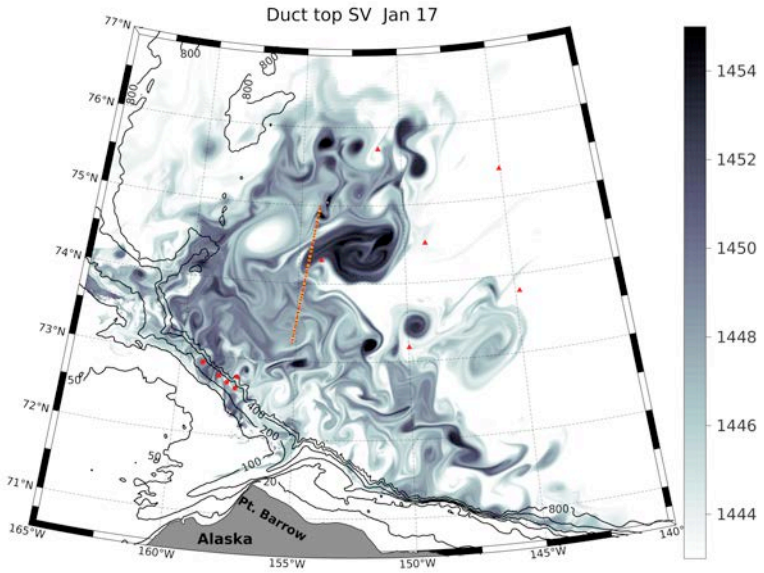

Fig 2: Modeled sound velocity (m/s) at the top of the PWW duct is shown for the Beaufort Gyre portion of the model. The color white is used where no duct is detected. Dark tint indicates very warm PSW and a substantial duct. The PWW layer and the Atlantic layer are relativly uniform, so the depicted duct-top sound velocity governs sound trapping. Also shown are a 200-km acoustic model track and CANAPE mooring stations.

2. REGIONAL OCEAN MODEL

To study the upper ocean conditions in the region, a high-resolution simulation was performed with the MITgcm primitive equation model. The model setup was patterned after that of Spall et al. [1], with some important changes. First, the horizontal resolution in the new model was much finer, with spacing of 500 m in much of the region. Next, the surface forcing was done using daily averages, updating each day, replacing monthly average forcing updated each month. The purpose of this is to widen the dynamic range of temporal response, which will produce an entirely different flow structure. The model was initialized with climatic PCHG3.0 climatological conditions that do not include much PSW and essentially no duct. The model is run with 2016 forcing (1 Jan to 31 Dec) that is repeated for three years. After a 720-day spin up, 375 days of model state were saved for analysis.

Fig. 2 shows the sound velocity at the duct top on day 748 of the run (Jan. 17). The dark areas show where two summers of PSW introduction into the area have built a duct. The PSW enters from the coastal current flowing eastward along the north shore of Alaska, then moves clockwise around the gyre. The western part of the Beaufort Gyre (west of 155W) contains a largely uninterrupted duct. Between 150 and 155 W, that filaments of colder water at the

density of the PSW disrupt the duct continuity. East of 150 W PSW is scarce and there will only be sound ducting in isolated patches.

The sound speed in the density layers above the PWW duct core is the primary variation in the ducting geometry in the model results, but there are other variations. Fig. 3 shows the duct sound speed versus density along one transect (a southward continuation of the 200-km track of Fig. 2). The warm upper duct boundary PSW layer lies at potential density 26.1 to 26.3 kg/m^3. The sound-speed $c(x,z,t)$ structure below the PWW duct is relatively uniform. The duct center, with minimum sound speed with respect to depth or density, is near 26.8, and has sound speed variations (temperature and salinity variations). Fig. 3c shows that salinity controls density at these temperatures, so that temperature is somewhat passive dynamically in the gyre, and that sometimes there is little or no signature of warm PSW which determines the existence of the duct. The intrusion of PSW and the stirring of PSW along isopycnals are processes that respond to density patterns created by surface forced circulation.

Fig. 4 shows the April 11 duct $c(x,z)$ more conventionally. In addition, the duct parameter $P=\Delta c\Delta z$ is plotted, where Δc is c at the duct top minus c at its minimum in the duct, and Δz is the height of the duct between the depths where c is maximum above the duct and where c rises again, below the duct, to that maximum value. Fig. 4 also shows variability of $P(x,t)$ along this line, and the cumulative distribution of log$P$ scaled against a normal distribution. The plot indicates that the duct is present about 70% of the time. Analysis shows that the correlation length scale of P is 26.5 km, and the length scale for duct-top c is 30 km.

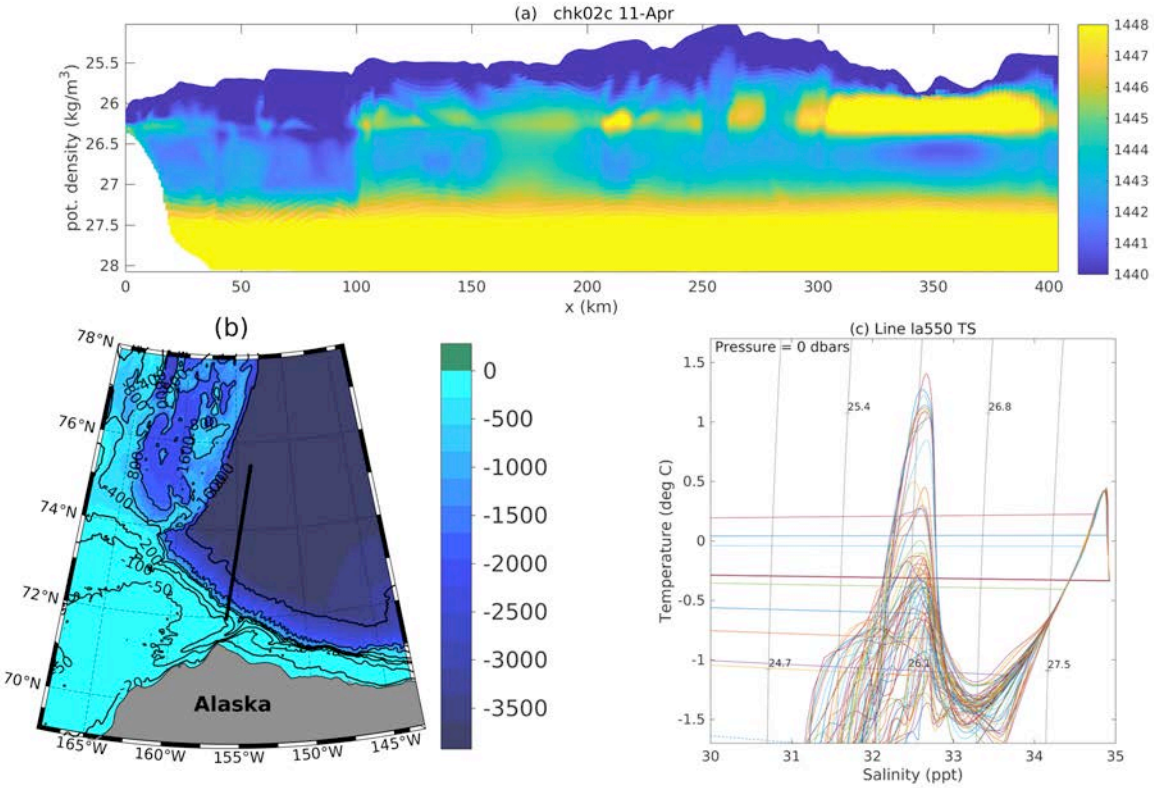

Fig. 3: (a) The sound velocity is plotted versus potential density re 0 dbar and distance along a line (550) of the MITgcm model grid. Range zero is at the south. Speed above 1448 m/s is color saturated. (b) The bathymetry of the area and the postion of line 550 are drawn. (c) The TS properties of a sequence of profiles are shown. Selected potential density contours are drawn. In (a), note that the duct upper cap (sound-speed maximum) is absent at 90 km. The sound-speed minimum in the duct is variable.

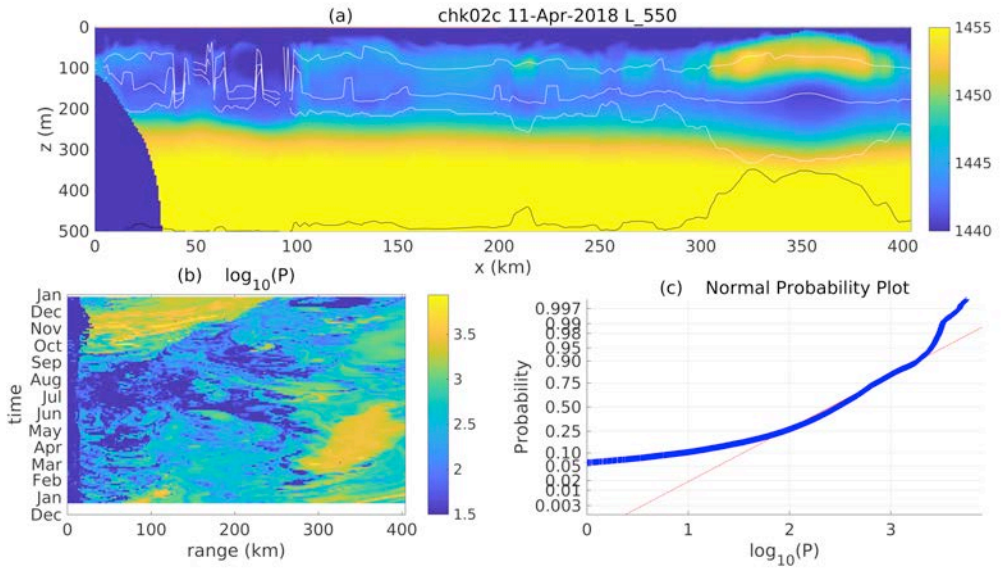

Fig. 4: (a) The sound speed in the duct of April (Fig. 3a) is plotted vs depth and distance. At the bottom, the duct parameter P(x) is plotted, multiplied -0.05 to fit onto the plot, with P=0 at 500 m depth (i.e. P=2000 would be at 400). (b) $Log_{10}(P(x,t))$ on the same transect is plotted for 375 days. (c) A probability plot of the cumulative distribution of $log_{10}(P)$ shows lognornal behavior from P=100 to P=2000. A weak duct would have P=(150 m)(1 m/s)=150, so the plot shows that 30% of the samples show no duct (P < 150).

3. SOUND PROPAGATION MODELING

Sound propagation modeling at 200 Hz was done with a parabolic equation (PE) technique that we have already applied to this area [2]. Most simulations have the source in the duct at 173-m depth, the same as used in CANAPE for sources moored in deep water. Initial results show that the sound in the duct is weakly affected by ice cover. When present, the ice strongly attenuates all other (not PWW ducted) sound. The effects of rough-underside ice on sound are approximately incorporated into the PE method using the equivalent fluid half-space complex-density method [4]. The half space approximation means that reflections from the surface are disregarded. The important interference effect that will occur with a uniform thickness ice layer will not be included, but with rough ice the disregarded interference will be random, so neglecting the surface boundary in that case should have relatively less error in the modeled ice reflectivity. The minimum nominal reflections coefficient of the ice lower surface is about 0.25 at 30° grazing angle.

Fig. 5 shows modeled sound in the duct versus range for a “broken duct” where a section of the PSW layer has a section that is too cold to form an effective duct. The function $\Psi(x, z)$ from the cylindrically symmetric PE is shown [5], which does not account for cylindrical spreading. The modeling was done with ice that has small background roughness plus ice keels. One of the primary results here is that ducted sound is converted to surface interacting sound when the layer at density 26.2 is not warm enough to create a duct (i.e. lacks sufficient PSW water). With no ice cover, the sound levels far from source may not be affected by this, but the sound energy may be reduced with ice above due to poor reflection, or to reflection to high angle from tilted ice, which will send sound into the seabed. All of these effects have been seen in our numerous simulations with variable ice and duct properties.

CANAPE data show surface interacting ~200-Hz sound to gradually lose intensity 220-km from a source at a rate of about 10 dB/month after ice appears in November. On the other

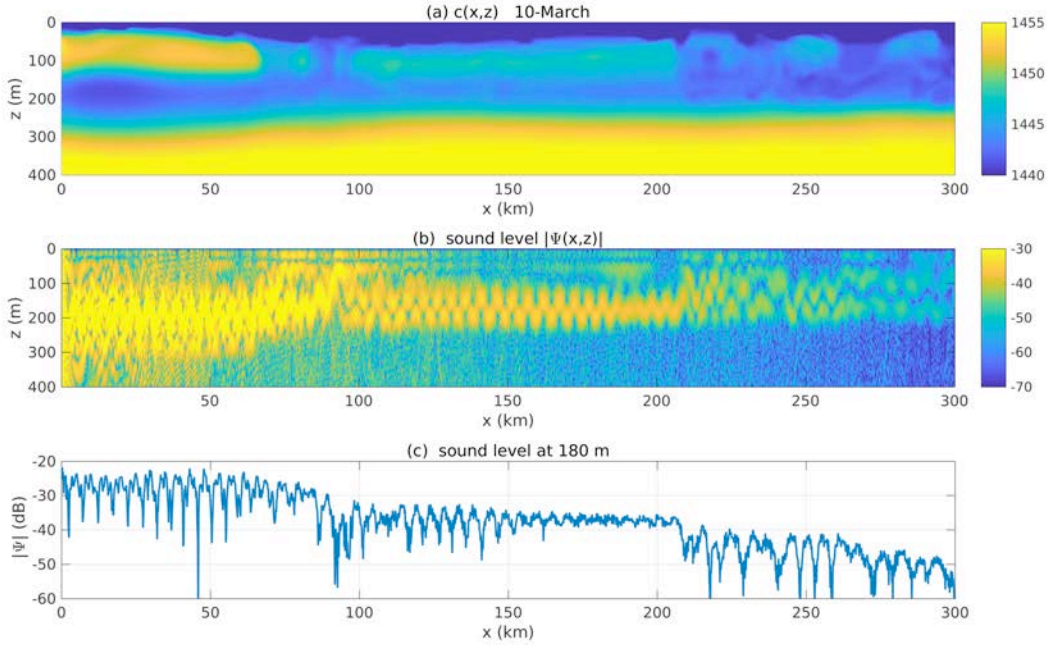

Fig. 5: (a) Sound speed in the upper layers is shown. Breaks in the PSW layer that affect sound trapping occur at x equals 85, 207 and 261 km. (b) Sound field intensity $|\Psi(x, z)|$ re 0 dB source is plotted. High intensity is color saturated. (c) Intensity at 180 m depth in the duct.

hand, identified ducted sound retains its energy until March, with a few brief interruptions, then it loses 45 dB in less than a month. To determine whether ice cover could reduce the level of ducted sound, range-independent simulations were performed with two ducts, weak and strong (Fig. 6) taken from the MITgcm output, and many ice conditions. Selected results are shown in Table 1. No simulations showed attenuation of the ducted sound equal to what was seen in the field. The surface-interacting sound was highly attenuated by the ice, as expected (not shown). For the simulations, ice was given a background roughness with Gaussian height distribution ranging from 0 to 4 m rms, with horizontal scales restricted from 4 m to 100 m wavelength. Some simulations had a synthesized set of ice keels added to flat surface with a very small roughness. The keel geometry followed statistics measured in the area at the time of CANAPE by the Beaufort Gyre Exploration Project [6] with upward looking ice sonars. The keel height distribution was near exponential, the half-width to depth ratio was 4.85 [7], and there were 4.1 keels per km. Keels deeper than 8 m numbered about one per 2 km.

Waveguide model	*400-km ducted TL, dB, cyl. spread. removed*
No ice	34
R-indep strong duct, flat ice	35
R-indep strong duct, rough ice	35
R-indep weak duct, flat ice	37.5
R-indep weak duct, keel model 1 ice	40
R-indep weak duct, rough ice	52

Table 1: Transmission loss (TL) for range-independent modeling of ducted 200-Hz sound. The effect of the ice cover on ducted sound at 400 km is a maximum of 18 dB loss. Cylindrical spreading loss is not included (10 $\log_{10}$ 40 km, 56 dB). Fig. 6 shows the ducts. Ducted sound level is computed with a 30-km long, 100-200 m depth incoherent average. The rough ice case is unrealistic and its attenuation exceeds that of keels.

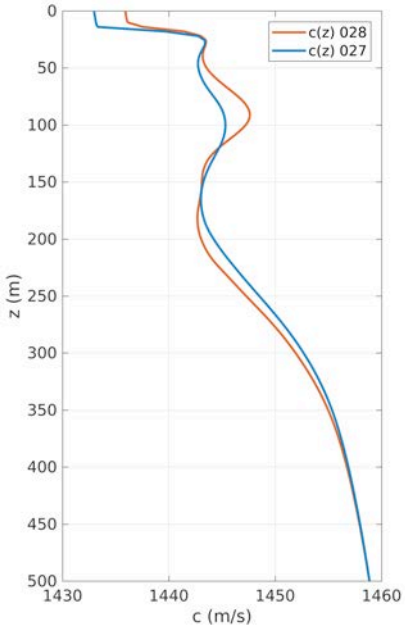

Fig. 6: Sound-speed profiles for range-independent weak duct (027) and strong duct (028) propagation modeling. See Table 1.

Finally, simulations were performed with range-dependent duct conditions taken from the hydrodynamic model. Result from two full-year, 400-km simulations are shown in Fig. 7, along the same north-to-south track used in the other simulations. The simulations have the same ice year-round (artificially), with one having the same ice keel statistics as used in the range-independent study (Table 1), and the other having scaled-down keel heights. Up to 35 dB of sound level reduction is seen as the PSW layer changes over the winter and spring.

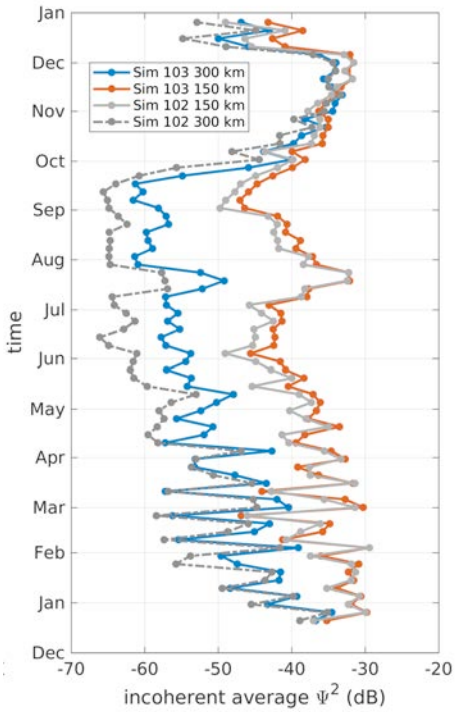

Fig 7: Sound level over one-year of simulations with keel ice above the time-dependent range-dependent conditions taken from the regional model. The track line is shown in Fig. 3b. The 200 Hz source is at 173 m depth at the north end.

4. SUMMARY

Sound propagation in the Beaufort Sea has been modeled using conditions taken from a surface-forced regional hydrodynamic model of the region. The propagation model includes a method to simulate the attenuating effects of ice. The field-observed effect that motivates this work is the reduction of sound trapped in the Pacific Winter Water sound duct. In the model, the duct has intermittent gaps that causes sound to escape from the duct and interact with the surface, resulting in up to ~35 dB reduction of sound intensity relative to an intact duct situation. Range-independent modeling was used to show that sound in an uninterrupted duct can also suffer loss from ice, but the loss only exceeds 10 dB for unrealistically rough ice. The results imply the 45 dB attenuation observed in the experiment requires the duct to be interrupted; ice loss alone is not of this magnitude. The broken-duct effect is insensitive to the detailed nature of the ice scattering and loss mechanisms. On the other hand, effects of ice on unducted sound may be more sensitive to the ice attenuation because that is the primary cause of time-dependent attenuation.

5. ACKNOWLEDGEMENTS

This work was funded by the US Office of Naval Research Ocean Acoustics Program. The regional model was run at a US Department of Defense High Performance Computing Facility, computing access was arranged through ONR. The Beaufort Gyre water-column data data were collected and made available by the Beaufort Gyre Exploration Program based at the Woods Hole Oceanographic Institution (https://www.whoi.edu/beaufortgyre) in collaboration with researchers from Fisheries and Oceans Canada at the Institute of Ocean Sciences. The parabolic model code was adapted from a Matlab version of the acoustic code RAM. The Matlab version is from M. Dzieciuch of UCSD.

REFERENCES

[1] **Spall, M. A., R. S. Pickart, M. Li, M. Itoh, P. Lin, T. Kikuchi, and Y. Qi, Y.,** Transport of Pacific Water into the Canada Basin and the formation of the Chukchi Slope Current, *J. Geophys. Res.,* volume 123, pp. 7453-7471, 2018.

[2] **Duda, T. F.,** Acoustic signal and noise changes in the Beaufort Sea Pacific Water duct under anticipated future acidification of Arctic Ocean waters, *J. Acoust. Soc. Am.,* volume 142, pp. 1926-1933, 2017.

[3] **Beaufort Gyre Exploration Project,** CTD and Geochemistry Data, 2017, https://www.whoi.edu/website/beaufortgyre/data

[4] **Zhang, Z. Y. and C. T. Tindle,** Improved equivalent fluid approximations for a low shear speed ocean bottom, *J. Acoust. Soc. Am.,* volume 98, pp. 3391-3396, 1995.

[5] **Jensen, F. B., W. A. Kuperman, M. B. Porter and H. Schmidt,** *Computational Ocean Acoustics,* 2nd Edition, Springer, 2011. (Chapter 6)

[6] **Beaufort Gyre Exploration Project**, https://www.whoi.edu/website/beaufortgyre/home

[7] **Kuuliala, L., P. Kujala, M. Suominen, and J. Montewka,** Estimating operability of ships in ridged ice fields, *Cold Regions Science and Technology*, volume 135, pp. 51-61. 2017.